Image Anal Stereol 2024;43:195-201 doi: 105566/ias.3078
Original Research Paper

AN EXPERIMENTAL STUDY FOR THE EFFECTS OF NOISE ON HYPERSPECTRAL IMAGERY CLASSIFICATION

GUANG YI CHEN✉,[1], ADAM KRZYZAK[1] AND SHEN-EN QIAN[2]

[1]Department of Computer Science and Software Engineering, Concordia University, Montreal, QC, Canada H3G 1M8; [2]Space Science and Technology, Canadian Space Agency, St-Hubert, QC, Canada J3Y 8Y9
e-mail: guang_c@cse.concordia.ca; krzyzak@cse.concordia.ca; shen-en.qian@asc-csa.gc.ca
(Received November 7, 2023; revised June 9, 2024; accepted June 12, 2024)

ABSTRACT

Hyperspectral image (HSI) classification is a very important topic in remote sensing. There are many published methods for HSI classification in the literature. Nevertheless, it is not clear which method is the most robust to noise in HSI data cubes. In this paper, we conduct a systematic study to examine the effects of noise in HSI data cubes on classification methods. We compare ten existing methods for HSI classification when Gaussian white noise (GWN) and shot noise are present in the HSI data cubes. We have figured out which method is the most robust to GWN and shot noise respectively by experimenting on three widely used HSI data cubes. We have also measured the CPU computational time of every method compared in this paper for HSI classification.

Keywords: edge preserving features; hyperspectral image classification; minimum noise fraction; principal component analyses; support vector machine.

INTRODUCTION

Classification of remote sensing images goes a long way to improve the performance of remote sensing. Information contents of hyperspectral images is significantly higher than that of conventional remote sensing images, especially in the spectral domain. The acquisition of hyperspectral images depends on imaging spectrometers installed in different spaces. The imaging spectrum was established in the 1980s in the ultraviolet, visible, near-infrared, and mid-infrared regions of electromagnetic waves. Since the imaging spectrometer can image in many continuous and very narrow bands, each pixel in the used wavelength range can get a fully reflected or emitted spectrum. As a result, hyperspectral images have the characteristics of high spectral resolution, many bands, and abundant information.

In this paper, we conduct a systematic study to understand how noise in hyperspectral imagery (HSI) affects image classification. We compare ten existing methods for HSI classification when Gaussian white noise (GWN) and shot noise are present in the HSI data cubes. We have determined which method is the most robust to GWN and to shot noise by experimenting on three widely used HSI data cubes.

The organization of this paper is as follows. Section II briefly reviews ten existing methods for HSI classification. Section III conducts experiments to determine which method is most robust to noise. Finally, Section IV concludes the paper and proposes future research directions.

THE COMPARED METHODS

We briefly review eleven popular methods for HSI classification here.

1. Tu *et al*. (2018) propose a new classifier based on correlation coefficient (CC) which can efficiently capture similarity among different pixels using combining CC and a joint sparse representation (JSR), with the latter one attempting to utilize the within-class similarity between training and test samples while reducing the between-class interference. This classification algorithm is called CCJS. It proceeds first by calculating CCs among the training and test samples and then uses the JSR-based classifier to produce the representation residuals of different pixels. The balance between the JSR and the CC is achieved by introducing a regularization parameter λ. The proposed algorithm demonstrates the competitive edge over other commonly used classifiers in experiments on the Indian Pines data set. In this paper, this classification method will be designated as CCJS.
2. Li *et al*. (2018) suggested reducing the spectral dimension of the hyperspectral images by combining a segmented principal component analysis (SPCA) and

the Gaussian pyramid decomposition-based multiscale feature fusion. The method works as follows: first spectral dimension reduction is accomplished by the SPCA and subsequently, the multiscale features are extracted from the resulting dimension-reduced image by Gaussian pyramids. Finally, SPCA is invoked again to compute Gaussian pyramid features (SPCA-GPs). The performance of SPCA-GPs is evaluated by using a support vector machine (SVM) classifier. In this paper this method will be designated as gp_hqb.

3. Kang *et al*. (2014) proposed an original spectral-spatial classification algorithm based on edge-preserving filtering. The proposed framework is made of three stages. In the first stage, the hyperspectral image is classified by a pixelwise classifier such as, a SVM classifier yielding a multiple probability map. In the second stage edge-preserving filtering is performed on each probability map with the first principal component or the first three principal components of the hyperspectral image playing the roles of the gray or color guidance image. In the third stage the class of each pixel is determined by the maximum probability. In this paper this method will be designated as EdgeP.

4. Kang *et al*. (2018) developed a new spectral-spatial classification algorithm based on Gabor filtering and deep network (GFDN). Gabor features are obtained by performing Gabor filtering on the first three principal components of the hyperspectral image. These components typically represent the low-level spatial structures of different orientations and scales. The Gabor features and spectral features are simply stacked to form the final fused features. Next, deep features are extracted by training a stacked sparse and deep autoencoder network which is supplied the fused features on its input. To overcome the problem of limited number of training hyperspectral image samples they are augmented by automatically generated virtual samples and both real and virtual samples are used in training parameters of the deep network to improve its classification accuracy. In this paper this method will be designated as GFDN.

5. Kang *et al*. (2015) introduced a novel spectral-spatial classification method for HSI based on extended random walkers (ERWs). In the first stage of this approach a SVM classifier is applied to classify hyperspectral image probability maps and yielding probability distributions of class membership for each hyperspectral pixel. In the second stage the pixelwise probability maps are optimized with the ERW algorithm by encoding the spatial information of the HSI in a weighted graph and the class of a test pixel is determined by three factors, namely the pixelwise statistics information learned by the SVM classifier, the spatial correlation among adjacent pixels yielded by the weights of graph edges, and finally by the connectedness information between the training and test samples modeled by random walkers. In this paper this method will be designated as iidf.

6. Spatial-aware collaborative representation (CR) is proposed for HSI classification in Jiang *et al*. (2017). A closed-form solution using spatial-spectral information has been proposed. That approach utilizes both spatial and spectral features by introducing the distance-weighted spatial regularization terms. The proposed approach outperforms the state-of-the-art classifiers in experiments on three HSI data sets. In this paper this method will be designated as JSaCR.

7. Kang *et al*. (2017) developed a novel algorithm for HSI classification by utilizing principal component analysis (PCA)-based Edge-Preserving Features (PCA-EPFs). The algorithm works as follows. First, the standard EPFs are derived by applying edge-preserving filters with different parameter settings to the input image and are subsequently stacked together. Next, spectral dimension of the stacked EPFs is reduced with the PCA, which not only represent the EPFs in the mean square sense but also emphasize the separability of pixels in the EPFs. Finally, the resulting PCA-EPFs are classified by an SVM classifier. In this paper, this method is designated as PCA_EPF.

8. Chen (2021) developed a novel algorithm for HSI classification based on PCA and SVM. He used PCA to reduce the dimensionality of an HSI data cube, and then performed spatial convolution with three different filters on the PCA output cube. He fed all three convolved output cubes to SVM to classify every pixel. Finally, he fused the three output maps to determine the final classification map. The experiments conducted on three widely used HSI data cubes (i.e., Indian Pines, Pavia University, and Salinas) demonstrate that the proposed method significantly outperforms state-of-the-art methods in terms classification accuracy. In this paper this method is be designated as MultiScalePCA.

9. Chen *et al*. (2021) introduced a novel approach for HSI classification by fusing PCA, 2D spatial convolution, and SVM. The proposed method takes advantages of correlation in both spatial and spectral domains in an HSI data cube. First, PCA is used to reduce the dimensionality of an HSI data cube and then spatial convolution is applied to dimension-reduced data cube twice in a sequence resulting in generating

two convolved PCA output data cubes in a multiresolution way. The two convolved data cubes are fed to the SVM to classify each pixel to one of the known classes. Experiments on three widely used hyperspectral data cubes (i.e., Indian Pines, Pavia University and Salinas) demonstrate significant improvement of the classification accuracy of the proposed approach over a few competing methods. This method will be designated as PCA+SVM.

10. Chen *et al*. (2022) proposed a new method for HSI classification by using minimum noise fraction (MNF), spatial filtering, and support vector machine (SVM). They consider the three most popular DR methods: PCA, minimum noise fraction (MNF), and locally linear embedding (LLE), which are applied to perform dimensionality reduction of a hyperspectral data cube before performing classification. Subsequently, 2D spatial filtering is applied to the DR output band images and then the pixels of the data cube are classified by the SVM. Thus, both spatial information and spectral information are involved in classification. Experimental results show that the proposed MNF+SVM approach decisively outperforms several existing classification methods. In this paper, this method is designated as MNF+SVM.

11. Chen *et al*. (2023) proposed the noise robust hyperspectral image classification with MNF-based edge-preserving features. In this method, we replaced PCA with MNF and better classification results were obtained for hyperspectral image classification. We do not compare this method in this paper, and we leave it to our future research.

RESULTS AND DISCUSSION

We test three HSI data cubes for HSI classification, which can be described as follows.

a. Indian Pines. This data cube was acquired by the airborne visible/infrared imaging spectrometer (AVIRIS) sensor over the Indian Pine test site in northwestern Indiana, USA, on June 12, 1992. The dimension of this data cube is 145×145 pixels and it has 200 spectral bands. Table 1 tabulates ground truth classes and the pixel number for every class in this data cube.

Table 1. *Ground truth classes and the total pixel number for each class in Indian Pines data cube.*

No	Class Names	Total Samples
C1	Alfalfa	46
C2	Corn notill	1428
C3	Corn mintill	830
C4	Corn	237
C5	Grass pasture	483
C6	Grass trees	730
C7	Grass pasture mowed	28
C8	Hay windrowed	478
C9	Oats	20
C10	Soybean notill	972
C11	Soybean mintill	2455
C12	Soybean clean	593
C13	Wheat	205
C14	Woods	1265
C15	Buildings Grass Trees Drives	386
C16	Stone Steel Towers	93

b. Pavia University. This data cube was collected by the ROSIS sensor during a flight campaign over Pavia, northern Italy, on July 8, 2002. The dimension of this data cube is 610×340 pixels and it has 115 spectral bands. There are 9 classes of land covers, which are tabulated in Table 2.

Table 2. *Ground truth classes and the total pixel number for each class in Pavia University data cube.*

No	Class Names	Total Samples
C1	Asphalt	6631
C2	Meadows	18649
C3	Gravel	2099
C4	Trees	3064
C5	Painted metal sheets	1345
C6	Bare Soil	5029
C7	Bitumen	1330
C8	Self-Blocking Bricks	3682
C9	Shadows	947

c. Salinas. This data cube was acquired by the AVIRIS sensor over Salinas Valley, California. The dimension of this data cube is 512×217 pixels it has 204 spectral bands. Table 3 shows ground truth classes and the total pixel numbers for all classes.

Table 3. *Ground truth classes and the total pixel number for each class in Salinas data cube.*

No	Class Names	Total Samples
C1	Broccoli green weeds 1	2009
C2	Broccoli green weeds 2	3726
C3	Fallow	1976
C4	Fallow rough plow	1394
C5	Fallow smooth	2678
C6	Stubble	3959
C7	Celery	3579
C8	Grapes untrained	11271
C9	Soil vineyard develop	6203
C10	Corn senesced green weeds	3278
C11	Lettuce romaine 4wk	1068
C12	Lettuce romaine 5wk	1927
C13	Lettuce romaine 6wk	916
C14	Lettuce romaine 7wk	1070
C15	Vinyard untrained	7268
C16	Vinyard vertical trellis	1807

In the experiments, Gaussian white noise (GWN) is added to the noise-free HSI data cubes with noise standard deviation σ_n=100, 200, 300, 400, and 500. A noisy hyperspectral imagery data cube can be generated by adding GWN to a noise-free data cube:

$$B=A+\sigma_n Z, \quad (1)$$

where Z obeys normal distribution with zero mean and unit variance, A is the noise-free data cube, B is the simulated noisy data cube, and σ_n is the noise standard deviation.

We also conduct experiments with shot noise added to the noise free data cubes by using the following Matlab command:

$$B(i) = \text{imnoise}(A(i),'\text{poisson}'), \quad (2)$$

where A(i) is the i=th noise-free spectral band of the HSI data cube and B(i) is the noisy spectral band after adding shot noise. Shot noise does not have a noise level in generating noisy data cube, which is totally different from the GWN.

Tables 4-6 show the overall classification accuracy (%) for the Indian Pines data set, the Pavia University data set, and the Salinas data set with GWN and shot noise, respectively. The best results are highlighted in bold font. In our experiments, we select 10% of samples as training data set for the Indian Pines data set, and we pick 2% of samples as training data set for the Pavia University data set and the Salinas data set. All the rest samples are for the testing data set. It can be seen from the tables that for GWN the JSaCR method performs the best for the Indian Pines data set, both the gp_hqb method and the GFDN method obtain the best results for the Pavia University data set, and the gp_hqb method achieves the best results for the Salinas data set. When there is no noise, the PCA_EPF method performs the best for the Indian Pines data set, the GFDN method obtains the best results for both the Pavia University data set and the Salinas data set. For shot noise, the JSaCR method performs the best for the Indian Pines data set and for the Pavia University data set, and the gp_hqb method achieves the best results for the Salinas data set. Fig. 1 shows the original noise-free band (#50) from the Pavia University data set and the noisy bands with different noise levels (σ_n=100, 200, 300, 400, 500) whereas Fig.2 displays the noise-free band and that with shot noise added.

Table 4. *Overall classification accuracy (%) for the Indian Pines data set with GWN and shot noise. The best results are highlighted in bold font.*

Methods	No Noise	GWN (σ_n)					Shot Noise
		100	200	300	400	500	
CCJS	95.33	94.34	93.98	93.63	93.09	91.54	33.22
gp_hqb	98.91	98.64	98.23	98.07	97.82	97.85	94.25
EdgeP	93.65	65.98	57.41	52.17	51.41	49.29	23.96
GFDN	98.57	98.46	98.41	98.45	97.86	98.27	95.13
iidf	97.17	88.97	80.21	75.00	69.54	65.65	23.96
JSaCR	98.67	**99.03**	**99.04**	**98.95**	**98.83**	**98.73**	**98.12**
PCA_EPF	**99.08**	97.77	96.87	96.48	95.88	95.61	66.41
MultiScalePCA	98.48	96.85	96.62	95.99	95.33	94.48	80.77
PCA+SVM	81.71	78.87	75.75	72.38	69.51	67.44	31.13
MNF+SVM	98.39	96.76	94.13	92.76	91.35	90.07	80.39

Table 5. *Overall classification accuracy (%) for the Pavia University data set with GWN and shot noise. The best results are highlighted in bold font.*

Methods	**No Noise**	**GWN (σ_n)**					**Shot Noise**
		100	**200**	**300**	**400**	**500**	
CCJS	83.90	66.65	57.39	53.67	52.53	50.70	38.59
gp_hqb	99.62	**99.75**	**99.72**	99.68	**99.66**	**99.63**	84.66
EdgeP	96.90	89.28	84.87	82.93	77.60	77.02	43.60
GFDN	**99.76**	**99.75**	**99.72**	**99.74**	99.65	99.52	80.66
iidf	99.26	99.18	97.39	93.20	90.26	86.78	2.21
JSaCR	98.44	97.97	96.83	95.43	94.06	92.86	**92.78**
PCA_EPF	98.81	98.78	98.52	98.59	98.48	98.47	90.34
MultiScalePCA	97.10	95.73	94.10	92.34	90.70	89.34	44.46
PCA+SVM	92.92	87.22	82.51	79.48	77.06	75.33	43.04
MNF+SVM	97.32	96.16	95.08	93.51	91.65	89.87	37.44

Table 6. *Overall classification accuracy (%) for the Salinas data set with GWN and shot noise. The best results are highlighted in bold font.*

Methods	**No Noise**	**GWN (σ_n)**					**Shot Noise**
		100	**200**	**300**	**400**	**500**	
CCJS	94.57	80.80	67.16	50.04	28.81	17.64	22.78
gp_hqb	99.78	**99.85**	**99.87**	**99.74**	**99.74**	**99.74**	**97.92**
EdgeP	95.68	86.54	80.91	71.80	60.65	59.47	20.82
GFDN	**99.81**	99.74	99.71	99.64	99.50	99.32	90.86
iidf	99.39	98.06	92.98	89.76	86.50	84.23	3.34
JSaCR	99.35	98.02	96.75	95.41	94.32	93.30	96.74
PCA_EPF	99.70	99.63	99.49	99.17	99.33	99.07	91.53
MultiScalePCA	98.67	94.96	91.38	89.31	87.80	86.45	23.33
PCA+SVM	94.50	84.49	78.06	74.59	72.13	70.14	18.05
MNF+SVM	98.74	95.08	94.66	93.64	93.01	92.25	40.00

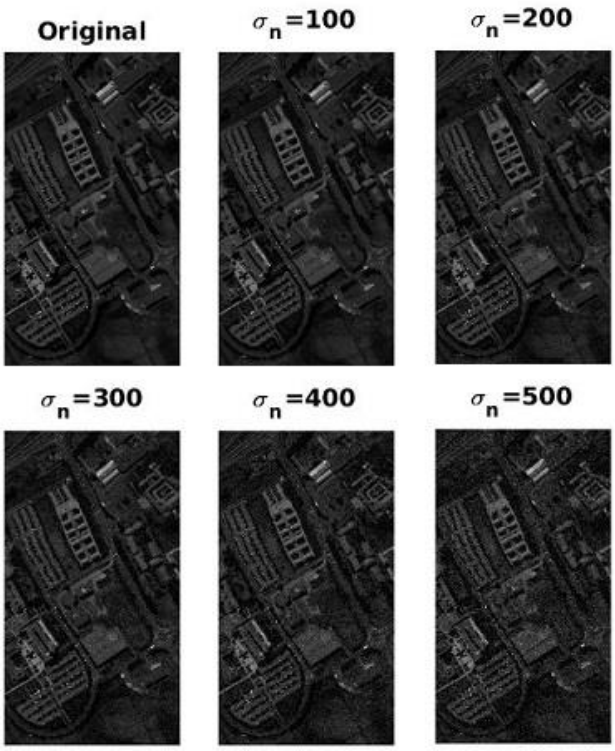

Fig. 1. *The noise-free #50 band in the Indian Pines data cube and the noisy spectral bands with GWN added.*

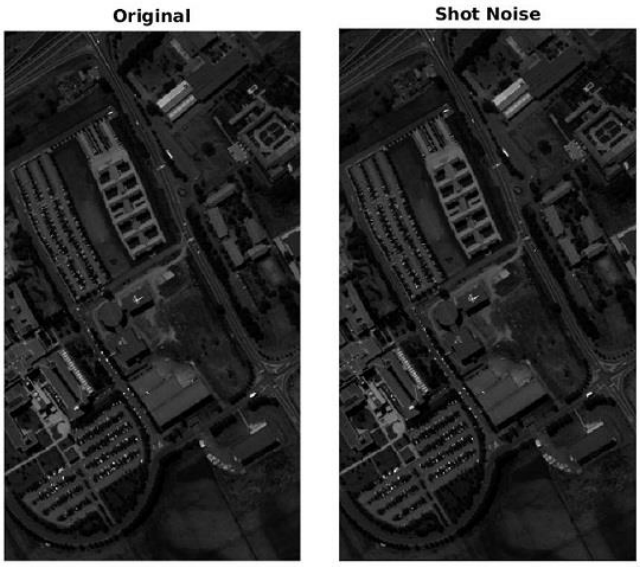

Fig. 2. *The noise-free #50 band in the Indian Pines data cube and the noisy band with shot noise added.*

Table 7 shows the execution time in seconds by using our unoptimized Matlab code for the Indian pines data cube, the Pavia University data cube, and the Salinas data cube. Our experiments are done under the Linux operating system with Intel(R) Xeon(R) CPU E5-2697 v2 at 2.70GHz and 131 GB of random-access memory (RAM). Our method MNF+SVM is the fastest for the Indian Pines data cube and the Pavia University data cube and PCA_EPF is the fastest for the Salinas data cube. The JSaCR method is the slowest among all methods compared in this paper. Nevertheless, it achieves very good classification results under the noisy environment for hyperspectral imagery classification.

Table 7. *The execution time in seconds by using our unoptimized Matlab code for the Indian pines data cube, the Pavia University data cube, and the Salinas data cube. The best results are highlighted in bold font.*

Method	**Indian Pines**	**Pavia University**	**Salinas**
CCJS	617.2	1830.6	3227.9
gp_hqb	121.1	**72.6**	113.2
EdgeP	468.3	119.7	382.8
GFDN	120.2	207.2	219.0
iidf	200.8	1487.8	876.9
JSaCR	631.8	2476.9	5592.8
PCA_EPF	72.9	73.9	**83.0**
MultiScalePCA	48.4	397.7	518.7
PCA+SVM	35.8	306.0	377.3
MNF+SVM	**7.7**	**72.6**	141.6

CONCLUSIONS

Classification of remotely sensed images is to identify and classify the information of the earth's surface and its environment on the remotely sensed images, so that we can identify the feature information corresponding to the image information and extract the required feature information. Classification of remotely sensed images is the specific application of automatic pattern recognition technology in the field of remote sensing.

In this paper, we have conducted a systematic study on HSI classification methods to examine the effects of noise in HSI data cubes on the classification. We have found out that the JSaCR method, the GFDN method, and the gp_hqb method are most robust to both GWN and shot noise. Nevertheless, the JSaCR method is the slowest in term of CPU computational time.

Future research will be done in the following ways. We may perform PCA-based denoising methods (Chen and Qian (2011), Chen *et al*. (2014), Luo *et al*. (2014)) for HSI image classification as a preprocessing step. We may investigate deep learning for HSI classification soon. Also, we may use low-rank matrix approximation for HSI classification. Furthermore, it is important to take advantages of both spatial and spectral information for HSI classification.

CONFLICT OF INTEREST

The authors declare that they have no conflict of interest.

ACKNOWLEDGEMENT

The authors would like to thank Dr. Xudong Kang and Dr. Shutao Li for providing their Matlab code of the PCA-EPFs method. We thank all other authors for their publicly available Matlab codes. Without these Matlab codes, this work could not have been done. The authors also thank the anonymous reviewer for his/her valuable comments, which improved the quality of this paper.

Data sharing is not applicable to this article as no datasets were generated or analyzed during the current study.

REFERENCES

Chen GY (2021), Multiscale filter-based hyperspectral image classification with PCA and SVM, Electr Eng, 72:40-5.

Chen GY Bui TB Quach KG and Qian SQ (2014), Denoising hyperspectral imagery using principal component analysis and block matching 4D filtering, Can J Remote Sens, 40:60-7.

Chen GY Krzyzak A and Qian SE (2022), Hyperspectral imagery classification with minimum noise fraction, 2D spatial filtering and SVM, Int J Wavelets Multi, 20:2250025.

Chen GY Krzyzak A and Qian S Q (2023), Noise robust hyperspectral image classification with MNF-based edge-preserving features, Image Anal Stereol, 42:93-9.

Chen GY and Qian SQ (2011), Denoising of hyperspectral imagery using principal component analysis and wavelet shrinkage, IEEE T Geosci Remote, 49:973-80.

Chen GY Xie WF Krzyzak A and Qian SE (2021), Hyperspectral image classification via principal component analysis, 2D spatial convolution, and support vector machines, J Appl Remote Sens, 15:032202.

Jiang J, Chen C, Yu Y, Jiang X, and Ma J, Spatial-aware collaborative representation for hyperspectral remote sensing image classification, IEEE Geosci Remote S, vol. 14, no. 3, pp. 404-408, 2017.

Kang X., Li S., Fang L, Li M and Benediktsson J A. (2015), Extended random walker-based classification of hyperspectral images, IEEE T Geosci Remote, 53:144-53.

Kang X, Li C, Li S and Lin H (2018), Classification of hyperspectral images by Gabor filtering based deep network, IEEE J Sel Top Appl, 11:1166-78.

Kang X, Li S and Benediktsson, JA (2014), Spectral-spatial hyperspectral image classification with edge-preserving filtering, IEEE T Geosci Remote, 52:2666-77.

Kang X, Xiang X, Li S and Benediktsson JA (2017), PCA-based edge-preserving features for hyperspectral image classification, IEEE T Geosci Remote, 55:7140-51.

Li S, Hao Q, Kang X and Benediktsson JA (2018) Gaussian pyramid based multiscale feature fusion for hyperspectral image classification, IEEE J Sel Top Appl, 11:3312-24.

Luo GC, Chen GY, Tian L, Qin K and Qian SE (2016), Minimum noise fraction versus principal component analysis as a preprocessing step for hyperspectral imagery denoising, Can J Remote Sens, 42:106-16.

Tu B, Zhang X, Kang X, Zhang G, Wang J and Wu J (2018), Hyperspectral image classification via fusing correlation coefficient and joint sparse representation, IEEE Geosci Remote S, 15:340-4.